frontiers | Frontiers in Energy Research

TYPE Original Research
PUBLISHED 01 March 2023
DOI 10.3389/fenrg.2023.1140537

OPEN ACCESS

EDITED BY
Amrit Mukherjee,
University of South Bohemia in České Budějovice, Czechia

REVIEWED BY
Daomin Min,
Xi'an Jiaotong University, China
Chen Yang,
Beijing Institute of Technology, China

*CORRESPONDENCE
Jianwei Mi,
jwmi@xidian.edu.cn

SPECIALTY SECTION
This article was submitted to Process and Energy Systems Engineering, a section of the journal Frontiers in Energy Research

RECEIVED 09 January 2023
ACCEPTED 13 February 2023
PUBLISHED 01 March 2023

CITATION
Li X, Mi J, Zhang Y, Chen G, Fan G, Wang D and Du Y (2023), Current-injected photovoltaic array for concentrated space solar power station.
Front. Energy Res. 11:1140537.
doi: 10.3389/fenrg.2023.1140537

Current-injected photovoltaic array for concentrated space solar power station

Xintong Li[1], Jianwei Mi[1]*, Yiqun Zhang[1], Guangda Chen[1], Guanheng Fan[2], Dongxu Wang[1] and Yingchun Du[1]

[1]Key Laboratory of Electronic Equipment Structure Design, Ministry of Education, Xidian University, Xi'an, China, [2]Academy of Advanced Interdisciplinary Research, Xidian University, Xi'an, China

In this article, the power generation of a concentrated space solar power station (SSPS) is enhanced by current-injected total-cross-tied (TCT-CI) photovoltaic (PV) array. First, a mathematical model of the TCT-CI–connected PV array is established. Second, PV arrays with several common topologies and TCT-CI topology are simulated and analyzed using MATLAB/Simulink. At last, comparative experiments are conducted for TCT and TCT-CI–connected PV arrays under the condition of non-uniform light intensity distribution. The results of the above indicate the following: 1) TCT-CI–connected PV arrays reduce the difficulty of MPPT in concentrated SSPS, 2) TCT-CI–connected PV arrays increase the power generated in concentrated SSPS, and 3) TCT-CI–connected PV arrays are applicable for concentrated SSPS.

KEYWORDS

PV array, space solar power station, current inject, non-uniform light intensity distribution, total-cross-tied

1 Introduction

Energy resources in the world are becoming increasingly scarce with the development of world economy and increase in population. In this scenario, new energy has received extensive attention. Solar energy has a broader application prospect because it is pollution free, is inexhaustible, and has inexhaustible characteristics. Photovoltaic (PV) arrays at the ground are affected by climatic changes, day and night, geographical environment, and other factors, resulting in reduced power generation. In order to solve the disadvantages of PV power generation at ground level, researchers are beginning to focus on power generation from space—the space solar power station (SSPS) (Xja et al., 2021).

At present, researchers have proposed a variety of conceptual schemes of SSPS. These schemes can be divided into two types according to the form of sunlight collection by SSPS. The first type is the non-concentrated type, that is, sunlight directly shines on the photovoltaic array. This type includes the 1979 SPS Reference Concept, the "SunTower" SPS system (Mankins, 2002), Tethered-SPS (Sasaki et al., 2007), and such others. The second type is the concentrated type (Jin et al., 2016); due to the high cost of PV cells, researchers have proposed the concentrated type to reduce the area of the PV arrays. In the concentrated-type SSPS, sunlight shines on the photovoltaic array after the concentrator. This type includes SPS-ALPHA (MANKINS, 2013), integrated symmetrical concentrated architecture (ISC) (Jin and Huang, 2018), and SSPS-OMEGA (Fan et al., 2020).

Due to the structural characteristics and manufacturing errors of the concentrated SSPS, the light intensity distribution on the solar receiver is not uniform. The non-uniform light

intensity distribution can cause mismatch losses, reduce power generation, cause hot spot problems, and even cause damage to the PV array (Alanazi et al., 2022). Uneven light intensity distribution reduces the performance of PV arrays, which affects the power generation of SSPS. Now, we have to find a method suitable for SSPS to improve the performance of photovoltaic arrays under non-uniform light intensity distribution.

To reduce the impact of non-uniform light intensity distribution on PV arrays, many methods have been proposed.

The first method uses a different PV array topology. Instead of the traditional series–parallel (SP) configuration, new structures such as BL, HC, and TCT are adopted. In Jazayeri et al. (2014), under the SP, BL, and TCT configurations, PSCs were simulated using MATLAB/Simulink. In ElyaqoutiIzbaimBouhouch (2021), the electrical behavior of S, parallel (P), SP, TCT, BL, and HC connected PV arrays under different PSCs. The aforementioned literature shows that TCT PV array performs the best among several common configurations under non-uniform irradiation.

The second method is PV array reconfiguration (PVAR), which is based on the TCT topology (Qi, 2022). This method can be divided into two types, namely, static PVAR (SPVAR) and dynamic PVAR (DPVAR) (Krishna and Moger, 2018; Storey et al., 2014). DPVAR changes the electrical connection between PV modules to adapt to non-uniform light intensity distribution (Bularka and Gontean, 2017; Wang et al., 2012; Matam and Barry, 2018), whereas SPVAR changes the physical position of PV panels to create a uniform light intensity distribution (RaniIlango and Nagamani, 2013; Sahu and Nayak, 2016).

SPVAR requires rearranging the positions of the PV panels, which consumes a large number of transmission wires. DPVAR does not change the physical positions of the PV panels but relies on the switch matrix to change the electrical connection relationship until the optimal connection mode is found (NahidanNiroomand and Dehkordi, 2021).

In the concentrated SSPS, the physical position of the PV modules is fixed. Therefore, SPVAR cannot be applied here. Because DPVAR makes the system more expensive and complex (Belhachat and Larbes, 2021), this method is also unsuitable for concentrated SSPS.

In order to maximize the power generated, the maximum power point tracking (MPPT) method is required. The non-uniform light intensity distribution causes multiple peaks in the power–voltage (PV) curve of the PV array (Ahmad et al., 2017; Awan et al., 2022). Conventional MPPT algorithms, such as P&O (Salameh and Taylor, 1990; SantosAntunes et al., 2006) and conductance increment method (INC) (ElgendyZahawi and Atkinson, 2013; Liu et al., 2008), can usually only find the first peak close to the starting point of the PV curve. When light intensity distribution is non-uniform, it is possible that the first peak is the local MPP but not global MPP (GMPP) (Titri et al., 2017). To make the MPPT algorithm more accurate, smarter but complex MPPT control algorithms have been proposed, such as the gray wolf algorithm improved by the Levy flight (WangCai and Zeng, 2021), ant colony algorithm (ACO) (Chao and Rizal, 2021), hybrid global MPPT searching method (Rizzo and Giacomo, 2021), and genetic algorithm (GA) (Mohammad et al., 2015). Although the GMPP can be tracked using the aforementioned algorithm, this increases the difficulty and time of MPPT.

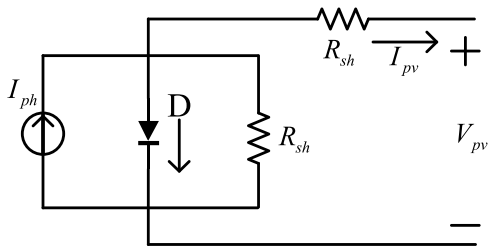

FIGURE 1
Model of a PV cell.

TABLE 1 Parameters of the PV model using Simulink.

Parameter	Value
P_m (W)	83.2848
N_{cell} (cells per module)	20
V_{oc} (V)	12.64
I_{sc} (A)	8.62
V_m (V)	10.32
I_m (A)	8.07
R_{sh} (ohms)	82.1161
R_s (ohms)	0.098625

To increase the output power of PV arrays in concentrated SSPS and reduce the difficulty of MPPT, the current injection TCT (TCT-CI) topology has been applied in this study. In the TCT-CI–connected PV array, each row is parallel with a controllable current source. Without considering the effect of light intensity from the PV module output voltage, each PV module can be operated at its GMPP.

In this article, Section 2 performs mathematical modeling on the PV cell and TCT-CI–connected PV array. Section 3 describes the evaluation method of PV array performance. Section 4 discusses and compares simulation results of the TCT-CI–connected PV array and other PV array configurations. In Section 5, comparative experiments are conducted for TCT and TCT-CI–connected PV arrays. Finally, Section 6 summarizes this whole article.

2 Mathematical modeling

PV arrays are connected by many PV cells. Commonly used PV cell models are single-diode models (Hasan and Parida, 2016).

As shown in Figure 1, the relationship between I_{pv} and V_{pv} (Mehta et al., 2019; Sai Krishna and Moger, 2019) is defined as

$$I_{pv} = I_{ph} - I_0\left[\exp\frac{q\left(V_{pv} + I_{pv}R_s\right)}{nKT} - 1\right] - \frac{V_{pv} + I_{pv}R_s}{R_{\mathrm{sh}}}, \quad (1)$$

where I_{ph} is the light generated current; I_0 is the diode's reverse saturation current; q is the electric charge on an electron, which is

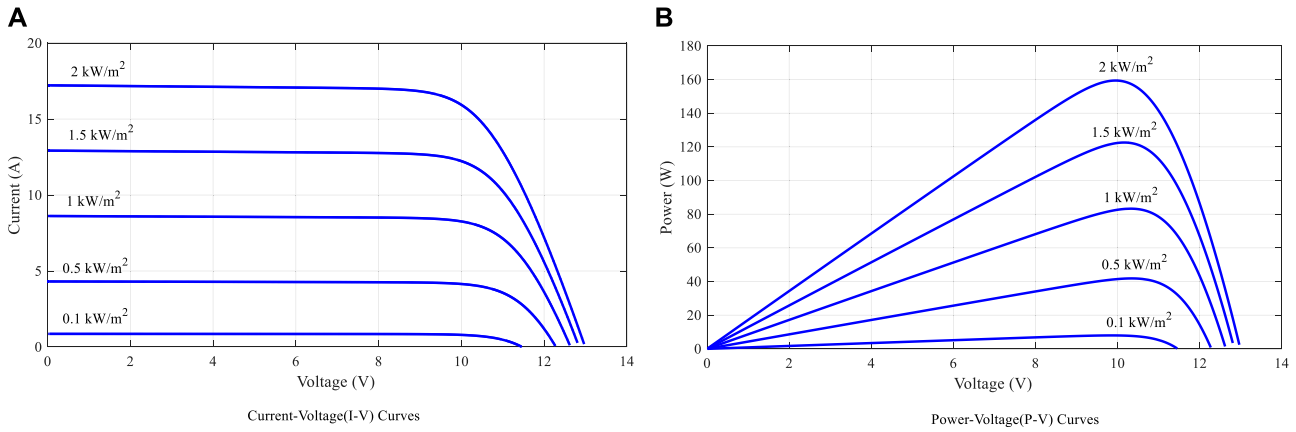

FIGURE 2
Characteristic curves for different irradiance levels. **(A)** I-V Curves, **(B)** P-V Curves.

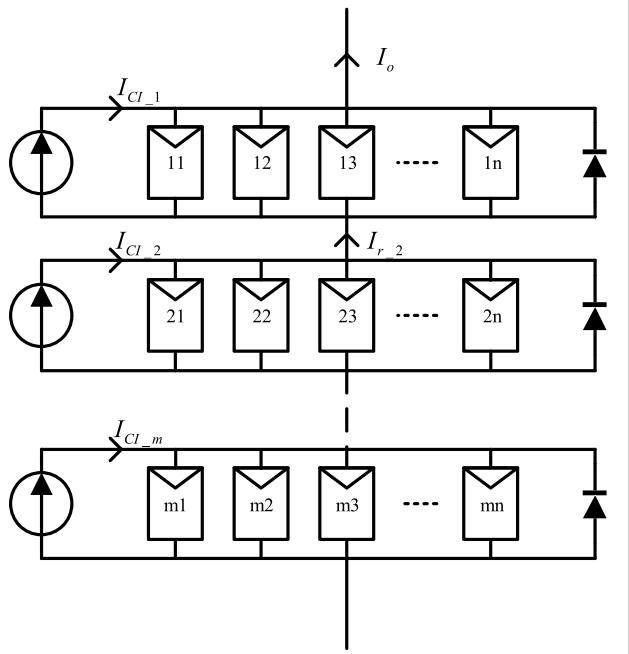

FIGURE 3
PV arrays with TCT-CI topology.

equal to 1.602176487*10^{-19}; n is the ideality factor; K is the Boltzmann's constant, which is equal to 1.3806504*10^{-23}; T is temperature in Kelvin, R_s is series resistance, and R_{sh} is shunt resistance. I_{sc} is the short-circuit current at the standard test condition (STC).

I_{ph} is proportional to solar irradiation(G) and temperature (T), which is defined as

$$I_{ph} = \frac{G}{G_o}\left[I_{sc} + K_{isc}\left(T - T_{STC}\right)\right], \tag{2}$$

where K_{isc} is the temperature coefficient of I_{sc}; G_0 is the light intensity under STC; T_{STC} is temperature under STC.

Parameters of the PV model used in Section 3/Simulink are shown in Table 1 and the PV curves are shown in Figure 2.

According to the I_{pv} and V_{pv} relationship, under constant temperature, I_{pv} is approximately proportional to the light intensity G and V_{pv} is approximately logarithmic to G. In concentrated SSPS, when PV modules are deployed, the same row of PV modules in the TCT-CI connected PV array are on the same horizontal line of the solar receiver. The light intensity distribution and temperature of PV modules in the same row is approximately the same, therefore the output voltages of PV modules in the same row are assumed to be the same.

When the temperature is constant, I_{pv} and V_{pv} are functions of G. In an $m \times n$ PV array (Figure 3), the light intensity on the module ij is G_{ij}, and then I_{pv} and V_{pv} at the GMPP of the module are expressed as follows:

$$\begin{cases} I_{ij} = I\left(G_{ij}\right) \\ V_{ij} = V\left(G_{ij}\right) \end{cases}. \tag{3}$$

In the TCT-CI topology, the output current in row k at GMPP is

$$I_{r\_k} = \sum_{j=1}^{n} I\left(G_{kj}\right), \tag{4}$$

and the output voltage in row k at GMPP is

$$V_{r\_k} = V\left(G_{ky}\right) \ (y \text{ is any integer between 1 and } n). \tag{5}$$

When the photoelectric effect of the PV modules in row k is weaker than that in other rows, the relative I_{r_k} is smaller. The parallel controlled current source operates in row k and injects current into it, such that its output current is equal to that in the other rows.

Under the action of controllable current sources, the output current of the array (I_o) is

$$I_o = \max\left[I_{r\_1}, I_{r\_2}, \ldots, I_{r\_m}\right]. \tag{6}$$

and the output voltage (V_o) is

$$V_o = \sum_{i=1}^{m} V_{r\_i}. \tag{7}$$

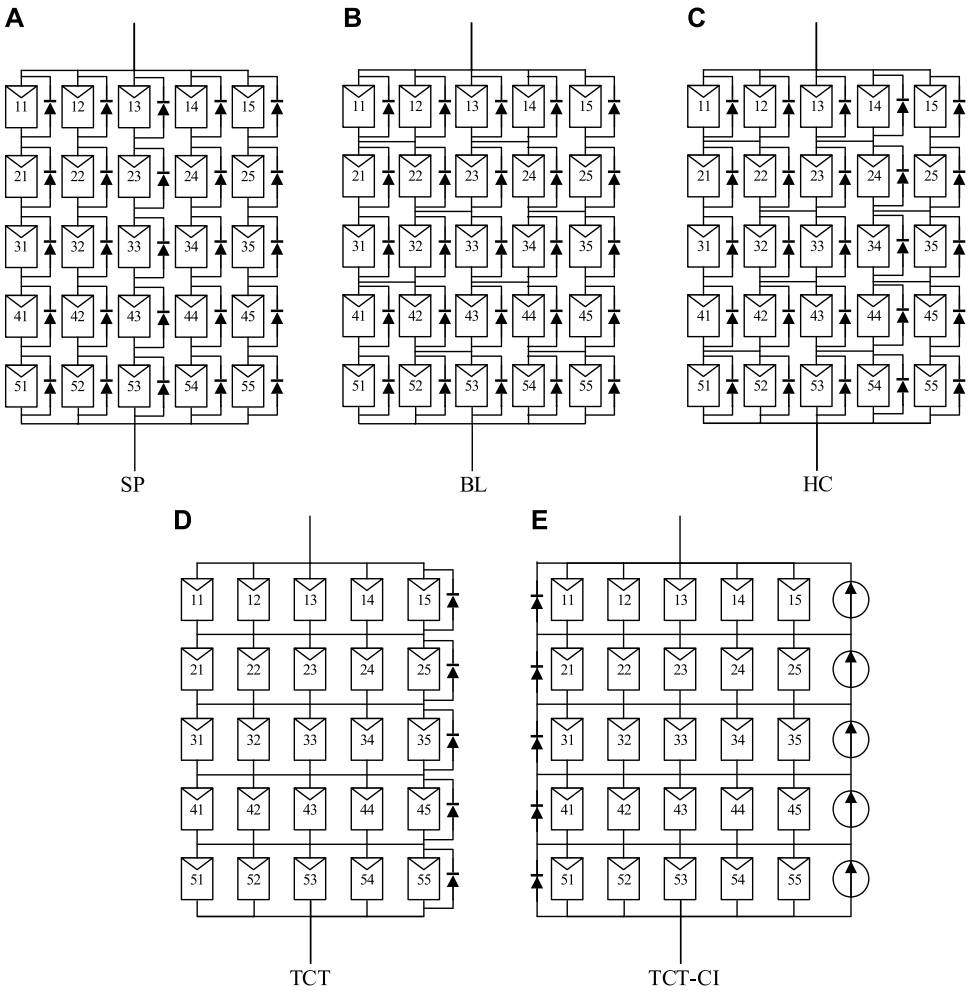

FIGURE 4
Several topologies of simulation. **(A)** SP, **(B)** BL, **(C)** HC, **(D)** TCT, **(E)** TCT-CI.

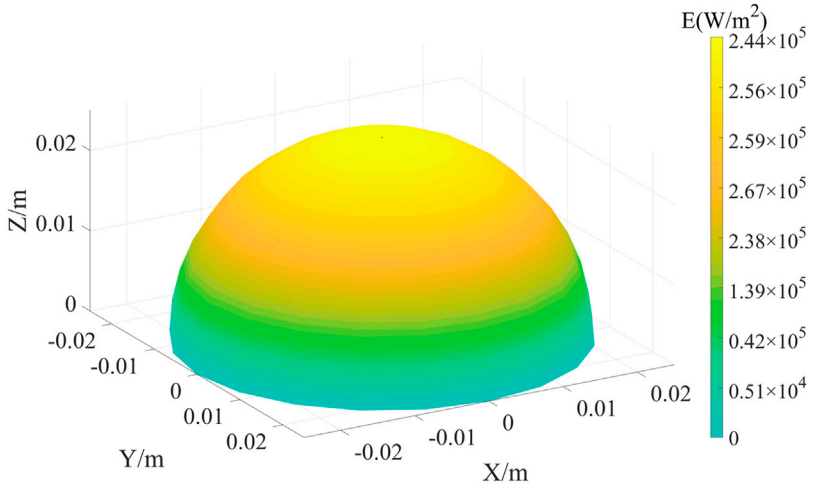

FIGURE 5
Flux density distribution of the hemisphere receiver with rotating parabolic concentrators (Liu et al., 2007).

10.3389/fenrg.2023.1140537

TABLE 2 Six irradiative conditions (units: W/m²).

	Column 1	Column 2	Column 3	Column 4	Column 5
(a) Case 1					
Row 1	1840	1904	2060	1834	2120
Row 2	2000	2164	2000	2132	2180
Row 3	1920	2140	2060	2186	1820
Row 4	1940	1898	1840	2140	1900
Row 5	2180	2194	2160	1956	2040
(b) Case 2					
Row 1	2320	1956	2380	2162	1700
Row 2	1700	1730	2380	2028	1740
Row 3	2240	2248	1700	2260	1820
Row 4	2000	1698	2140	2116	2000
Row 5	2260	1620	1660	2154	1660
(c) Case 3					
Row 1	2010	1924	1870	1876	2172
Row 2	1798	1789	1643	1757	1926
Row 3	1486	1573	1696	1755	1485
Row 4	1309	1431	1380	1498	1466
Row 5	1225	1105	1120	1288	1141
(d) Case 4					
Row 1	1640	2400	2268	2320	2036
Row 2	1822	1973	1739	1987	2128
Row 3	1514	1536	1293	1325	1616
Row 4	1310	1168	1282	1372	1235
Row 5	1099	1198	1130	991	1440
(e) Case 5					
Row 1	973	928	970	1017	934
Row 2	754	736	877	762	874
Row 3	607	564	613	564	554
Row 4	430	417	380	364	408
Row 5	212	211	202	192	210
(e) Case 6					
Row 1	1192	875	974	852	992
Row 2	797	868	701	682	666
Row 3	507	549	507	694	676
Row 4	435	374	399	435	458
Row 5	227	164	195	200	198

TABLE 3 Estimation of the TCT PV array.

Case	1	2	3	4	5	6
I_{TCT_out} (A)	78.424	75.487	47.442	47.277	23.411	23.668
P_{TCT} (W)	4046	3895	2448	2439	725	733
Short-circuited part	None	None	None	None	Rows 4 and 5	Rows 4 and 5

The output current of the controllable current source in row k (I_{CI_k}) is

$$I_{CI\_k} = \max[I_{r\_1}, I_{r\_2}, \ldots, I_{r\_m}] - I_{r\_k}. \tag{8}$$

The total output power of m controllable current sources is

$$\begin{aligned} P_{CI} &= \sum_{i=1}^{m} (V_{r\_i} \times I_{CI\_i}) \\ &= \sum_{i=1}^{m} (V_{r\_i} \times (\max[I_{r\_1}, I_{r\_2}, \ldots, I_{r\_m}] - I_{r\_i})). \end{aligned} \tag{9}$$

The output power of the array is

$$P_{TCT-CI} = V_o \times I_o - P_{TCT\_CI} = \sum_{k=1}^{m} \left(\sum_{j=1}^{n} I(G_{kj}) \cdot V_{r\_k} \right). \tag{10}$$

In practical applications, $\max[I_{r\_1}, I_{r\_2}, \ldots, I_{r\_m}]$ is obtained by measuring the currents of the bypass diodes and the output current of the array when the current injection section is not started.

According to Eqs 8–10, when the PV array has a TCT-CI topology, the working current of each row is the current at the GMPP, and there is no mismatch loss.

3 Evaluation of the PV array

When the irradiation is not uniform, the performance of the PV array can be evaluated from GMPP, mismatch power loss (MPL), power loss (PL), filling factor (FF), and efficiency (η).

3.1 Mismatch power loss

MPL refers to the difference between the sum of the maximum power of all PV modules in the PV array and the maximum power of the PV array under non-uniform light intensity. MPL can be determined as

$$\text{MPL} = \text{sum of all modules at MPP}_{\text{module}} - \text{GMPP}_{\text{non-uni}}. \tag{11}$$

The larger the MPL, the greater is the influence of the output power of the PV array with non-uniform irradiation.

3.2 Power loss

PL represents the difference between the global maximum power of the PV array under STC (1,000 W/m^2, AM1.5, 25°C) and that under non-uniform light intensity distribution. PL can be determined as

$$\text{PL} = \text{Power at MPP}_{\text{uni}} - \text{Power at GMPP}_{\text{non-uni}}. \tag{12}$$

Because the irradiation on the PV array in concentrated SSPS is not uniform, MPL is used in this study to measure the effectiveness of various configurations.

3.3 Filling factor

The product of I_{sc} and V_{oc} is the limit of the output power of the PV module. The ratio of the product of I_{sc} and V_{oc} to the global maximum power (P_m) is defined as the filling factor (FF).

$$\text{FF} = \frac{P_m}{V_{oc} \cdot I_{sc}} = \frac{V_m \cdot I_m}{V_{oc} \cdot I_{sc}}. \tag{13}$$

The larger the FF, the higher is the output power and efficiency of the photovoltaic module. FF affects the output efficiency of the PV module.

3.4 Photoelectric conversion efficiency (η)

When the photovoltaic module is exposed to light, the ratio of the output electric power to incident optical power is the photovoltaic conversion efficiency (η) of the photovoltaic module.

$$\eta = \frac{P_m}{P_{in}} = \frac{V_m \cdot I_m}{P_{in}} = \frac{FF \cdot V_{oc} \cdot I_{sc}}{P_{in}}, \tag{14}$$

where P_{in} is the incident optical power.

4 Simulation and analysis using MATLAB/Simulink

To prove the advantage of the TCT-CI–connected PV array in concentrated SSPS, this section simulates PV arrays with several common topologies and the TCT-CI topology (Figure 4). The PV array consists of 5 × 5 PV cells. The characteristic curves of the PV modules are shown in Figure 2.

The flux density distribution of the hemisphere receiver when the concentrator is a rotating paraboloid is shown in Figure 5. When the PV array is uniformly attached to the surface of the receiver, the light intensity distribution on the same row is approximately equal but different between the rows.

The six light intensity distributions used in the simulation are shown in Table 2, which are based on the light concentration characteristics of the abovementioned rotating parabolic concentrator. Cases 1, 2, and 3 had errors of 10%, and some others had errors of 20%. The PV array was evaluated in three

TABLE 4 Current values (units: A).

	Row 1	Row 2	Row 3	Row 4	Row 5
(a) In Case 1					
$I_{r\_i\_m}$	78.747	84.541	81.717	78.424	84.977
$I_{r\_i\_sc}$	84.114	90.303	87.286	83.769	90.769
(b) In Case 2					
$I_{r\_i\_m}$	84.880	77.294	82.863	80.329	75.487
$I_{r\_i\_sc}$	90.665	82.562	88.510	85.803	80.631
(c) In Case 3					
$I_{r\_i\_m}$	79.506	71.933	64.521	57.168	47.442
$I_{r\_i\_sc}$	84.924	76.835	68.919	61.064	50.675
(d) In Case 4					
$I_{r\_i\_m}$	86.058	77.859	58.775	51.383	47.277
$I_{r\_i\_sc}$	91.924	83.166	62.781	54.885	50.499
(e) In Case 5					
$I_{r\_i\_m}$	38.914	32.312	23.411	16.137	8.285
$I_{r\_i\_sc}$	41.566	34.514	25.007	17.237	8.849
(f) In Case 6					
$I_{r\_i\_m}$	39.422	29.962	23.668	16.957	7.949
$I_{r\_i\_sc}$	42.109	32.004	25.281	18.112	8.491

ways: global maximum power (GMP), mismatch loss (MPL), and filling factor (FF).

4.1 Estimation of power generation form TCT and TCT-CI–connected PV arrays

4.1 1TCT-connected PV arrays

In the PV array, if the output current of the array (I_{TCT_out}) is greater than the short-circuit current of a row ($I_{r\_i\_sc}$), the parallel bypass diode will be turned on and the row will be short-circuited. When estimating the GMP of the TCT-connected PV array, we should pay attention to whether a row is short-circuited by the bypass diode.

According to Eqs 1, 2 and Figure 2, when the temperature is at the standard test condition (STC), the output current at the GMPP is almost proportional to the light intensity, and the output voltage almost does not change with the change in light intensity.

I_m represents the current at the GMPP of the module under STC. $I_{r\_i\_m}$ is used to represent the current at the GMPP of row i under the existing irradiative condition. $I_{r\_i\_sc}$ is used to represent the short-circuit current of row i under the existing irradiative condition. In Case 1, $I_{r\_1\_m}$ and $I_{r\_i\_sc}$ are,

$$I_{r\_1\_m} = \left(\frac{1840}{1000}\right)I_m + \left(\frac{1904}{1000}\right)I_m + \left(\frac{2060}{1000}\right)I_m + \left(\frac{1834}{1000}\right)I_m + \left(\frac{2120}{1000}\right)I_m = 9.758I_m, \tag{15}$$

TABLE 5 Estimation of the TCT-CI PV array.

Case	1	2	3	4	5	6
P_{TCT_CI} (W)	4214.88	4136.92	3308.37	3316.47	1199.21	1188.12

TABLE 6 Parameters of the PV module for this experiment (STC).

Parameter	Valve
P_{mppt} (W)	3.6
V_{oc} (V)	6.6
I_{sc} (mA)	713
V_m (V)	5.6
I_m (mA)	642

$$I_{r\_1\_sc} = \left(\frac{1840}{1000}\right)I_{sc} + \left(\frac{1904}{1000}\right)I_{sc} + \left(\frac{2060}{1000}\right)I_{sc} + \left(\frac{1834}{1000}\right)I_{sc} + \left(\frac{2120}{1000}\right)I_{sc} = 9.758I_{sc}. \tag{16}$$

Same as the above, get row currents in the other cases, and substitute the values in Table 1 into Eqs 15, 16 to obtain $I_{r\_i\_m}$ and $I_{r\_i\_sc}$.

If $I_{TCT\_out} > I_{r\_i\_sc}$, row i will be short-circuited, and the PV modules in row i will not generate electricity.

In Case 1 and Case 2, the difference between the $I_{r\_i\_m}$ is not large, so no PV module will be short-circuited. The minimum of the row current values is chosen as I_{TCT_out}.

In Case 1,

$$I_{TCT\_out} = I_{r\_4\_m} = 78.424\text{A}, \tag{17}$$

$$P_{TCT\_out} = I_{TCT\_out} \times 5V_m = 4046\text{W}. \tag{18}$$

In Case 2,

$$I_{TCT\_out} = I_{r\_5\_m} = 75.487\text{A}, \tag{19}$$

$$P_{TCT\_out} = I_{TCT\_out} \times 5V_m = 3895\text{W}. \tag{20}$$

In Case 3,

a) If $I_{TCT\_out} = I_{r\_1\_m}$, rows 2, 3,4, and 5 will be short-circuited, and in this situation,

$$I_{TCT\_out} = I_{r\_1\_m} = 79.506\text{A}, \tag{21}$$

$$P_{TCT\_out} = I_{TCT\_out} \times V_m = 820\text{W}. \tag{22}$$

b) If $I_{TCT\_out} = I_{r\_2\_m}$, rows 3, 4, and 5 will be short-circuited, and in this situation,

$$I_{TCT\_out} = I_{r\_2\_m} = 71.933\text{A}, \tag{23}$$

$$P_{TCT\_out} = I_{TCT\_out} \times 2V_m = 1485\text{W}. \tag{24}$$

c) If $I_{TCT\_out} = I_{r\_3\_m}$, rows 4 and 5 will be short-circuited, and in this situation,

$$I_{TCT\_out} = I_{r\_3\_m} = 64.521\text{A}, \tag{25}$$

$$P_{TCT\_out} = I_{TCT\_out} \times 3V_m = 1998\text{W}. \tag{26}$$

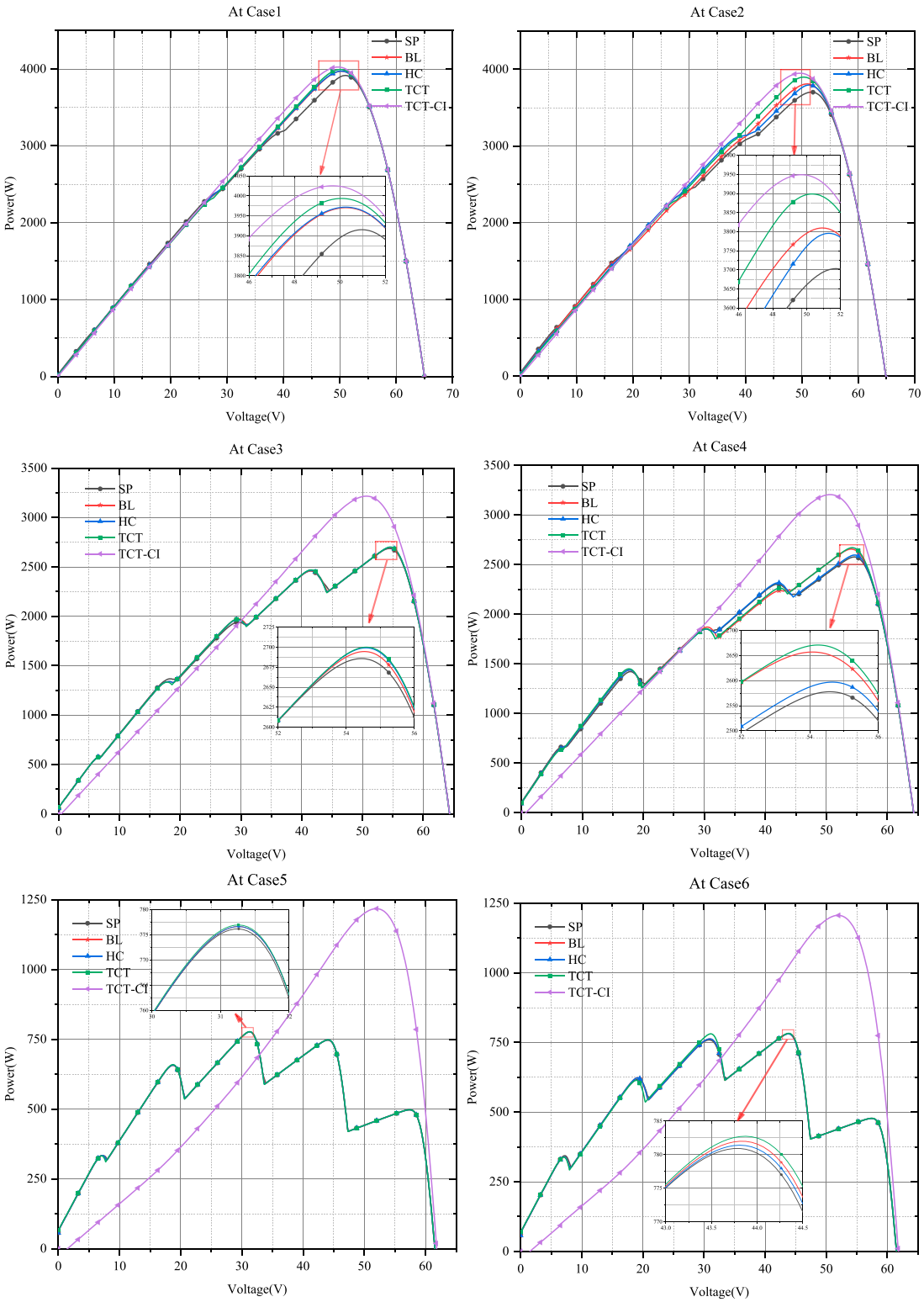

FIGURE 6
PV characteristic curves obtained by the simulation.

d) If $I_{TCT\_out} = I_{r\_4\_m}$, row 5 will be short-circuited, and in this situation,

$$I_{TCT\_out} = I_{r\_4\_m} = 57.168\text{A}, \tag{27}$$

$$P_{TCT\_out} = I_{TCT\_out} \times 4V_m = 2360\text{W}. \tag{28}$$

FIGURE 7
GMPP, MPL, and FF.

e) If $I_{TCT\_out} = I_{r\_5\_m}$, no PV model will be short-circuited, and in this situation,

$$I_{TCT\_out} = I_{r\_4\_m} = 47.442\text{A}, \tag{29}$$

$$P_{TCT\_out} = I_{TCT\_out} \times 4V_m = 2448\text{W}. \tag{30}$$

From a) to e), the value that makes P_{TCT_out} maximum is selected as I_{TCT_out}. So $I_{TCT\_out} = I_{r\_5\_m}$, and no PV model will be short-circuited.

Same as the above, P_{TCT} from the other cases is obtained. Results are shown in Table 3.

When $I_{r\_i\_m} < I_{TCT\_out} < I_{r\_i\_sc}$, the output voltage in row i is actually less than V_m. When $I_{TCT\_out} < I_{r\_i\_m}$, the output voltage in row i is actually greater than V_m and less than V_{oc}. Therefore, this subsection has some errors in estimating the generation of PV arrays but can correctly calculate whether PV modules are short-circuited.

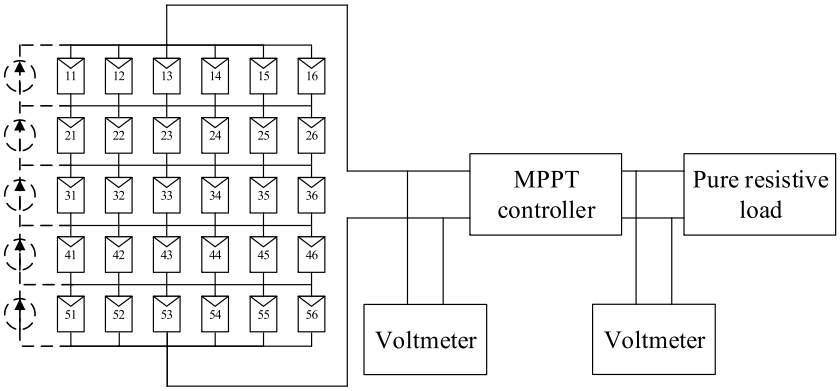

FIGURE 8
Schematic diagram.

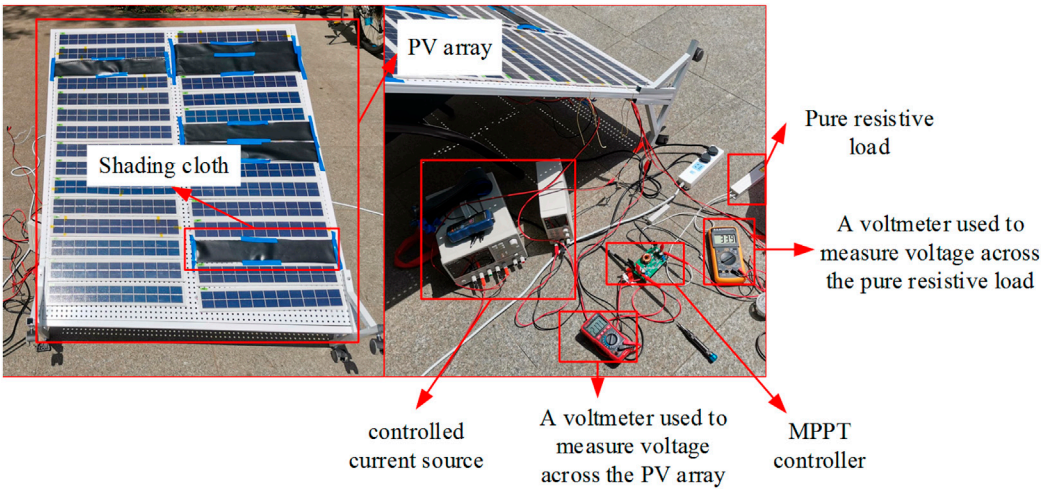

FIGURE 9
Real shooting of experiment.

4.1.2TCT-CI–connected PV arrays

Because of the controlled current source of the TCT-CI–connected PV array, each PV module can operate at the GMPP.

According to Table 4, in Case 1, the global maximum power of TCT-CI–connected PV array is defined as

$$P_{TCT\_CI} = (9.758I_m + 10.476I_m + 10.126I_m + 9.718I_m + 10.53)V_m = 50.608P_m = 4214.88\text{W}. \quad (31)$$

Same as the above, P_{TCT_CI} from the other cases is obtained. Results are shown in Table 5.

4.2 PV arrays' performance

The models were simulated using MATLAB/Simulink. The PV curves under the light intensity distribution are shown in Figure 6, and the MPL and filling factor are shown in Figure 7.

In Case 5 and Case 6, the output voltage at GMPP of the TCT-CI PV array is significantly greater than that of the others, indicating that some modules of the others are short-circuited by the bypass diode. This is consistent with the estimate in Section 4.1.

As shown in Figure 6, simulation results show that TCT-CI connected PV arrays have higher output power compared to other PV arrays. PV curves of TCT-CI connected PV arrays show a single peak. So conventional MPPT algorithms can be used here. PV curves of others PV arrays show multiple peaks. Conventional MPPT algorithms cannot track to GMPP, so more complex algorithm is required. Therefore, TCT-CI connected PV arrays reduce the difficulty of MPPT under non-uniform light intensity distribution. As shown by the polyline in Figure 7, the FF of TCT-CI connected PV arrays are slightly larger than that of others, and the MPL of TCT-CI connected PV arrays is 0.

In conclusion, TCT-CI–connected PV arrays have the following advantages under non-uniform illumination intensities:

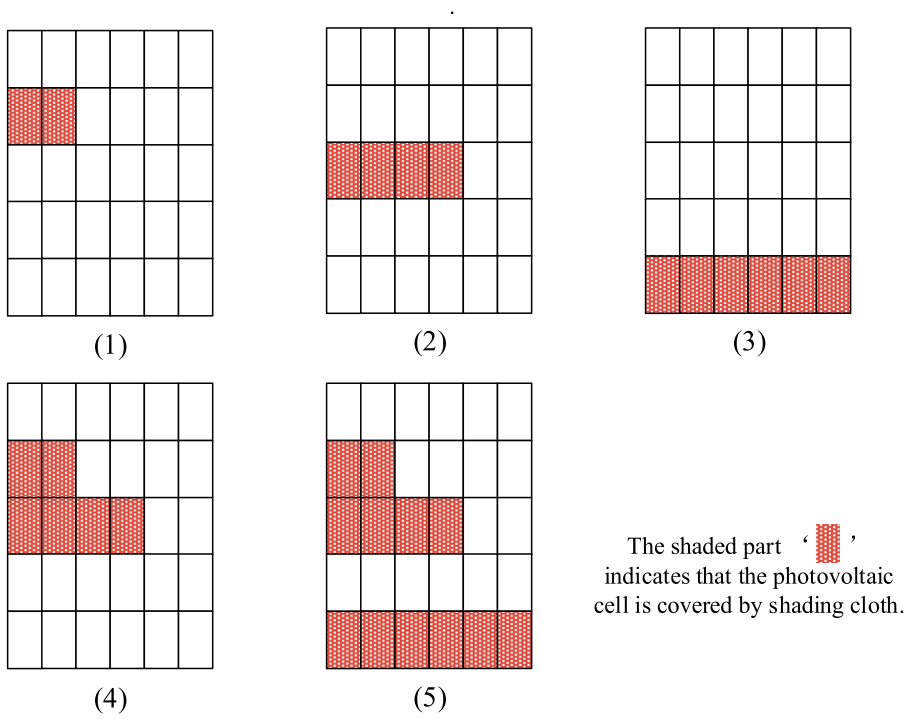

FIGURE 10
Shaded part.

TABLE 7 Comparison of experimental Data.

Shadow form	V_{oc} (V)		V_{mpp} (V)		V_{load} (V)		P_{CI} (W)	P_m (W)	
	TCT	TCT-CI	TCT	TCT-CI	TCT	TCT-CI	TCT-CI	TCT	TCT-CI
(1)	31.99	31.99	28.05	26.87	31.34	36.56	8.24	80.51	101.32
(2)	31.97	31.8	29.57	24.97	23.16	36.96	16.36	43.97	95.61
(3)	31.37	31.22	26.92	24.19	1.63	36.1	24.67	0.22	82.15
(4)	31.56	31.49	28.63	21.71	22.78	33.84	9.75	42.54	68.52
(5)	29.3	29.3	24.59	24.44	1.08	29.54	17.24	0.1	46.06

i. no mismatch loss,
ii. maximum GMPP,
iii. maximum photoelectric conversion efficiency,
iv. maximum filling factor and best performance, and
v. PV curve showing a single peak value, which reduces the difficulty of MPPT.

5 Experiment and analysis

To further verify that the TCT-CI–connected PV arrays are more suitable for concentrated SSPS, a comparative experiment between the TCT-CI and TCT-CI topologies was carried out. The experimental schematic is shown in Figure 8. The real shooting is shown in Figure 9. In the experiment, 30 photovoltaic models constituting 5*6 photovoltaic arrays were analyzed. Parameters of the PV module for this experiment at STC are shown in Table 6.

In Figure 8, the dashed line represents parallel controlled current sources. When the PV array is in the TCT topology, the controllable current source is not connected to the PV module. When the PV array is in the TCT-CI topology, the controllable current source is connected to the PV module as shown in Figure 8. During the experiment, the PV array was oriented toward the sun in such a way that sunlight was perpendicular to the PV module.

A pure resistive load was used in the experiment. In the TCT topology experiment, when the line loss was not considered, with the MPPT controller, the power consumed by the load (P_{load}) was the global maximum power (P_m) of the PV array. Therefore, P_m can be calculated by directly measuring the voltage across the load.

In the TCT-CI topology experiment, the external power supply was used as a controllable current source. Because the energy of the

external power supply is an external input, to obtain the global maximum power (P_m) of the PV array, the power of the external power supply (P_{CI}) has to be subtracted from the power consumed by the load (P_{load}). Then, the expression of P_m becomes

$$P_m = P_{load} - P_{CI}. \tag{32}$$

In the experiment, some photovoltaic modules were covered with a shading cloth to create a non-uniform light intensity distribution. Five groups of experiments were conducted, and the numbers and positions of the shading cloths are shown in Figure 10.

Because the basic light intensity did not change significantly during the experiment, the experimental results were not normalized; P_m of the PV arrays with TCT and TCT-CI topologies obtained in the experiment is shown in Table 7. It can be seen that under a non-uniform light intensity distribution, the global maximum power of the PV array with the TCT-CI topology is significantly larger than that with the TCT topology.

6 Conclusion

This study shows that the TCT-CI–connected PV array is suitable for concentrated SSPS. In the future, the following research has to be carried out: the existing TCT-CI–connected PV array uses a large number of controllable current sources, therefore the number of controllable current sources can be reduced in the next step.

This study analyzes and compares the performance of SP, BL, HC, TCT, and TCT-CI–connected PV arrays under non-uniform light intensity. Several PV arrays with different topologies were simulated by considering light intensity distribution in concentrated SSPS with rotating paraboloids as an example. Finally, comparative experiments on PV arrays with TCT and TCT-CI topologies were carried out. Both simulation and experimental results show that the PV array with TCT-CI topology has the best performance, and the difficulty of MPPT is reduced in non-uniform light intensity distribution.

In other words, PV arrays with TCT-CI topology are more suitable for concentrated SSPS, which can reduce the influence of non-uniform light intensity distribution on the performance of PV arrays.

Data availability statement

The original contributions presented in the study are included in the article/Supplementary Material; further inquiries can be directed to the corresponding author.

Author contributions

Drafting the manuscript: XL, JM, and YZ; critical revision of manuscript for important intellectual content: GC, GF, DW, and YD.

Funding

This work was supported by the Civil Aerospace Technology Research Project (D010103), the National Natural Science Foundation of China (Grant No. 52022075, Grant No. U1937202), and the National Key R&D Program of China (Grant No. 2021YFB3900300).

Conflict of interest

The authors declare that the research was conducted in the absence of any commercial or financial relationships that could be construed as a potential conflict of interest.

Publisher's note

All claims expressed in this article are solely those of the authors and do not necessarily represent those of their affiliated organizations, or those of the publisher, editors, and reviewers. Any product that may be evaluated in this article, or claim that may be made by its manufacturer, is not guaranteed or endorsed by the publisher.

References

Ahmad, R., Ali, F. M., Hadeed, A. S., Shami, U. T., and Saheed, O. (2017). An analytical approach to study partial shading effects on pv array supported by literature. *Renew. Sustain. Energy Rev.* 74, 721–732. doi:10.1016/j.rser.2017.02.078

Alanazi, M., Ahmed, F., Yousri, D., and Rezk, H. (2022). Optimal reconfiguration of shaded PV based system using African vultures optimization approach. *Alexandria Eng. J.* 61 (12), 12159–12185. doi:10.1016/j.aej.2022.06.009

Awan, M. M. A., Muhammad Yaqoob, J., Asghar, A. B., and Ejsmont, K. (2022). Performance optimization of a ten check MPPT algorithm for an off-grid solar photovoltaic system. *Energies* 15 (6), 2104. doi:10.3390/en15062104

Belhachat, F., and Larbes, C. (2021). Pv array reconfiguration techniques for maximum power optimization under partial shading conditions: A review. *Sol. Energy* 230, 558–582. doi:10.1016/j.solener.2021.09.089

Bularka, S., and Gontean, A. (2017). "Dynamic PV array reconfiguration under suboptimal conditions in hybrid solar energy harvesting systems," in *IEEE 23rd international symposium for design and Technology in electronic packaging (SIITME)* (IEEE).

Chao, K. H., and Rizal, M. N. (2021). A hybrid mppt controller based on the genetic algorithm and ant colony optimization for photovoltaic systems under partially shaded conditions. *Energies* 14, 2902. doi:10.3390/en14102902

ElgendyZahawi, M. A. B., and Atkinson, D. J. (2013). Assessment of the incremental conductance maximum power point tracking algorithm. *IEEE Trans. Sustain. Energy* 4 (1), 108–117. doi:10.1109/tste.2012.2202698

ElyaqoutiIzbaimBouhouch, M. D. L. (2021). Study of the energy performance of different PV arrays configurations under partial shading. *E3S Web Conf.* 229 (2), 01044. doi:10.1051/e3sconf/202122901044

Fan, G., Duan, B., Zhang, Y., Ji, X., and Qian, S. (2020). Thermal control strategy of OMEGA SSPS based simultaneous shape and topology optimization of butterfly wing radiator. *Int. Commun. Heat Mass Transf.* 119, 104912. doi:10.1016/j.icheatmasstransfer.2020.104912

Hasan, M. A., and Parida, S. K. (2016). An overview of solar PV panel modeling based on analytical and experimental viewpoint. *Renew. Sustain. Energy Rev.* 60, 75–83. doi:10.1016/j.rser.2016.01.087

Jazayeri, M., Uysal, S., and Jazayeri, K. (2014). *A comparative study on different photovoltaic array configurations under partial shading conditions* in 2014 IEEE PES T&D Conference and Exposition (Chicago, IL, USA: IEEE), 1–5.

Jin, H., Chu, X. M., Fan, J. Y., Jin, Q. B., and Duan, Z. Z. (2016). A novel concentrator with zero-index metamaterial for space solar power station. *Adv. Space Res.* 59 (6), 1460–1472.

Jin, Q. B., and Huang, J. (2018). The solar-tracking optimal trajectory planning research based on minimum energy consumption in SSPS. *Aerosp. Sci. Technol.* 76, 272–279. doi:10.1016/j.ast.2018.01.038

Krishna, G. S., and Moger, T. (2018). "SuDoKu and optimal SuDoKu reconfiguration for TCT PV array under non-uniform irradiance condition," in 2018 IEEE 8th Power India International Conference (PIICON) (IEEE).

Liu, F., Duan, S., Liu, B., Kang, Y., and Li, F. (2008). A variable step size inc mppt method for pv systems. *IEEE Trans. Industrial Electron.* 55 (7), 2622–2628. doi:10.1109/tie.2008.920550

Liu, Y., Dai, J., Lang, Z., and Xin, C. (2007). Finite-element analysis for flux distribution on focal plane of rotating parabolic concentrators. *Acta Opt. Sin.* 27 (10), 1775–1778.

Mankins, J. C. (2002). A technical overview of the "suntower" solar power satellite concept. *Acta Astronaut.* 50 (6), 369–377. doi:10.1016/s0094-5765(01)00167-9

Mankins, J. C. (2013). Sps-alpha: A novel approach to practical space solar power. *Ad Astra* 25 (1), 38–41.

Matam, M., and Barry, V. R. (2018). Variable size dynamic pv array for small and various dc loads. *Sol. Energy* 163, 581–590.

Mehta, H. K., Warke, H., Kukadiya, K., and Panchal, A. K. (2019). Accurate expressions for single-diode-model solar cell parameterization. *IEEE J. PVs* 9 (3), 803–810. doi:10.1109/jphotov.2019.2896264

Mohammad, S., Ahmadi, S., and Shirzad, A. (2015). A pso-based maximum power point tracking for photovoltaic systems under environmental and partially shaded conditions. *Prog. Photovoltaics* 23, 214. doi:10.1002/pip.2416

NahidanNiroomand, M. H. M., and Dehkordi, B. M. (2021). Power enhancement under partial shading condition using a two-step optimal pv array reconfiguration. *Int. J. Photoenergy* 2021, 1–19. doi:10.1155/2021/8811149

Qi, J. (2022). PV array reconfiguration according to shaded cells' number of every PV module. *CSEE J. Power Energy Syst.* doi:10.17775/CSEEJPES.2020.06140

RaniIlango, B. I. G. S., and Nagamani, C. (2013). Enhanced power generation from pv array under partial shading conditions by shade dispersion using su do ku configuration. *IEEE Trans. Sustain. Energy* 4 (3), 594–601. doi:10.1109/tste.2012.2230033

Rizzo, S. A., and Giacomo, S. (2021). A hybrid global MPPT searching method for fast variableshading conditions. *J. Clean. Prod.* 298. doi:10.1016/j.jclepro.2021.126775

Sahu, H. S., and Nayak, S. K. (2016). Extraction of maximum power from a pv array under nonuniform irradiation conditions. *IEEE Trans. Electron Devices* 63 (12), 4825–4831. doi:10.1109/ted.2016.2616580

Sai Krishna, G., and Moger, T. (2019). Improved SuDoKu reconfiguration technique for total-cross-tied PV array to enhance maximum power under partial shading conditions. *Renew. Sustain. Energy Rev.* 109, 333–348. doi:10.1016/j.rser.2019.04.037

Salameh, Z., and Taylor, D. (1990). Step-up maximum power point tracker for photovoltaic arrays. *Sol. Energy* 44 (1), 57–61. doi:10.1016/0038-092x(90)90027-a

SantosAntunes, J. L. F., Anis Chehab, C. C., and Cruz, C. (2006). A maximum power point tracker for pv systems using a high performance boost converter. *Sol. Energy* 80 (7), 772–778. doi:10.1016/j.solener.2005.06.014

Sasaki, S., Tanaka, K., Higuchi, K., Okuizumi, N., Kawasaki, S., Shinohara, N., et al. (2007). A new concept of solar power satellite: Tethered-SPS. *Acta Astronaut.* 60 (3), 153–165. doi:10.1016/j.actaastro.2006.07.010

Storey, J., Wilson Peter, R., and Bagnall, D. (2014). The optimized-string dynamic photovoltaic array. *IEEE Trans. Power Electron.* 29, 1768–1776. doi:10.1109/tpel.2013.2265497

Titri, S., Larbes, C., Toumi, K., and Benatchba, K. (2017). A new mppt controller based on the ant colony optimization algorithm for photovoltaic systems under partial shading conditions. *Appl. Soft Comput.* 58, 465–479. S1568494617302703. doi:10.1016/j.asoc.2017.05.017

Wang, Y., Xue, L., Chang, N., and Pedram, M. (2012). "Dynamic reconfiguration of photovoltaic energy harvesting system in hybrid electric vehicles," in *Proceedings of the 2012 ACM/IEEE international symposium on Low power electronics and design*, 109–114. ACM. doi:10.1145/2333660.2333688

WangCai, S. W., and Zeng, L. (2021). Research on mppt based on gray wolf algorithm improved by levy flight. *J. Phys. Conf. Ser.* 1865 (4), 042089. doi:10.1088/1742-6596/1865/4/042089

Xja, B., Bda, B., Yza, B., Gfa, B., Meng, L. C., and Yang, Y. D. (2021). Effect of operational condition of rotational subsystem on attitude control for space solar power station. *Chin. J. Aeronautics* 34 (5), 289–297. doi:10.1016/j.cja.2020.12.034